

Article

Doped Ruthenium/Hypercrosslinked Polystyrene (HPS) Catalysts in the Modification of Fatty Acid Methyl Esters

Romulo C. Dutra ¹, Thatiane V. S. Martins ², Delma da G. Rocha ², Mario R. Meneghetti ²,
Simoni M. P. Meneghetti ², Mikhail G. Sulman ^{3,4}, Valentina G. Matveeva ^{3,4} and Paulo A. Z. Suarez ^{1,*}

¹ Laboratory of Materials and Fuels, Chemistry Institute, University of Brasilia, Brasilia 70910-000, Brazil

² Group of Catalysis and Chemical Reactivity, Chemistry and Biotechnology Institute, Federal University of Alagoas, Maceio 57072-970, Brazil

³ Department of Biotechnology, Chemistry and Standardization, Tver Technical University, Tver 170026, Russia

⁴ Regional Technological Centre, Tver State University, Tver 170100, Russia

* Correspondence: psuarez@unb.br

Abstract: The modification of fatty substrates using heterogeneous catalysts have extensive industrial application and has an emphatic position in a sustainable context. Herein ruthenium, nickel, cobalt and copper-doped ruthenium, supported on hypercrosslinked polystyrene (HPS) catalysts were prepared by wet impregnation, characterized and applied on the modification of canola fatty acid methyl esters (FAME). The characterization showed a dispersive effect of doping metals over the ruthenium particles, the presence of acid sites and overall surface morphology, which allows targeting potential applications. The chosen modifications consisted of hydrogenation, hydroformylation, oxidative cleavage and deoxygenation, resulting in superb catalytic activities of over 99% conversions for hydrogenation and deoxygenation. The simplicity of the canola FAME composition allows the understanding of the catalytic processes and allows the upscale of more complex FAME matrixes. Finally, the obtained data stimulates further optimization studies for each application with a variation on the catalysts and the usage of residual fatty substrates, greatly enhancing the sustainability profile of the systems.



Citation: Dutra, R.C.; Martins, T.V.S.; Rocha, D.d.G.; Meneghetti, M.R.; Meneghetti, S.M.P.; Sulman, M.G.; Matveeva, V.G.; Suarez, P.A.Z. Doped Ruthenium/Hypercrosslinked Polystyrene (HPS) Catalysts in the Modification of Fatty Acid Methyl Esters. *Catalysts* **2023**, *13*, 630.

<https://doi.org/10.3390/catal13030630>

Academic Editor: Mauro Bassetti

Received: 6 February 2023

Revised: 7 March 2023

Accepted: 16 March 2023

Published: 21 March 2023



Copyright: © 2023 by the authors. Licensee MDPI, Basel, Switzerland. This article is an open access article distributed under the terms and conditions of the Creative Commons Attribution (CC BY) license (<https://creativecommons.org/licenses/by/4.0/>).

Keywords: ruthenium; doped; catalyst; hypercrossed polystyrene; heterogenized; FAME

1. Introduction

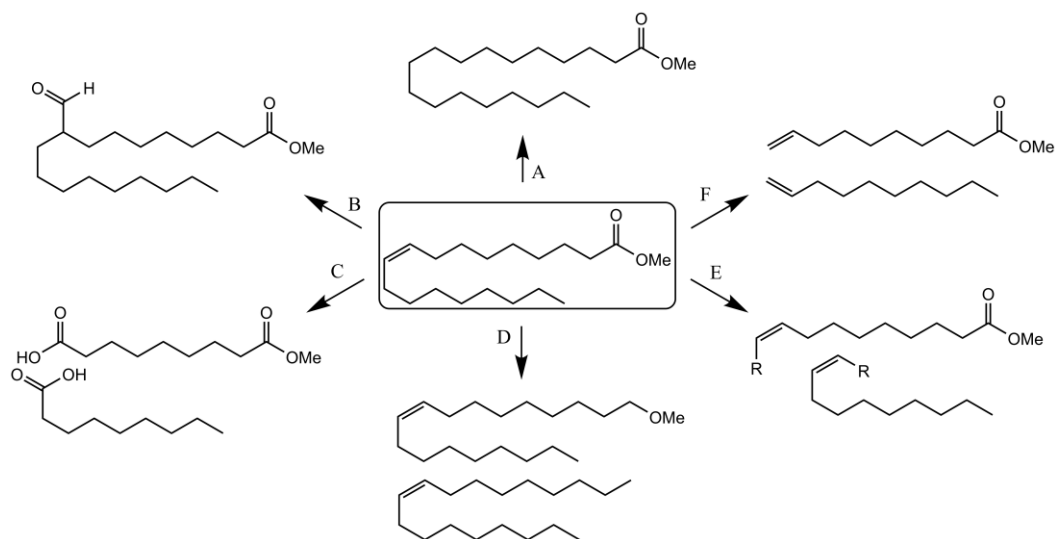
Heterogeneous catalysis plays a prominent role due to its great advantages compared to homogeneous ones, because they are usually easy to regenerate and reuse, exhibiting thermal, chemical and structural stability in addition to being low cost. However, some disadvantages must be considered, such as the complexity of active sites, leaching and limited surface-substrate contact [1–3].

One area in which the use of heterogeneous catalysts has emerged is that of functionalization of fatty substrates, mainly by their simple operation, requiring less unitary operations for product isolation, and results in products exhibiting high purity with increased value, which may be characterized as a circular economy and biorefinery application [4–6].

The unsaturations in fatty acids chains are active sites for a large range of reactions, which could be employed to modify biodiesel characteristics such as the cold-flow properties, besides making it possible to prepare value-added derivatives with a wide range of applications such as additives, plasticizers, lubricants, detergents, surfactants, polymer precursors, etc. In addition, since allylic hydrogens are susceptible to radical attack and consequent oxidative degradation, the removal of unsaturations permits to improve the product's oxidative stability.

Some modifications plausible for fatty substrates (Scheme 1) include, among others, hydrogenations (A), hydroformylations (B), oxidative cleavages (C), deoxygenations (D), metathesis (E) and ethenolysis (F) [7–10]. The hydrogenation process is still used for

the production of hydrogenated fats using nickel Raney, but can also be accomplished using, bimetallic ruthenium-nickel supported over molecular sieves and others [11–13]. The hydroformylation processes normally occur by homogeneous catalysis but may proceed using rhodium or ruthenium heterogenized over MOFs, functionalized silica and others [14,15]. The oxidative cleavage process uses ozonolysis, but may also be accomplished using ruthenium catalysts and composites of ruthenium-vanadium heterogenized and others [16–18]. The deoxygenation of fatty compounds is an efficient route for green diesel production using heterogenized catalysts supported on zeolites and others [19–21].



Scheme 1. Products from different modification routes of the methyl oleate: (A) hydrogenation; (B) hydroformylation; (C) oxidative cleavage; (D) deoxygenation; (E) metathesis and (F) ethenolysis.

Hypercrosslinked polystyrenes (HPS), or functionalized polystyrenes (such as amine-functionalized), are useful in the stabilization of metallic nanoparticles and clusters [22–25]. The stabilization of nanoparticles is vital for the production of ruthenium mono and bimetallic catalysts applicable in biorefinery processes, such as the oxidation and hydrogenation of glucose, the hydrogenolysis of cellulose, on Suzuki cross-coupling and on the lactic acid hydrogenation [26–28].

In this work, the synthesis and characterization data of the ruthenium, and doped ruthenium/HPS (5%Ru/HPS and 3%Ru-0.1%Me/HPS; Me = Co, Ni and Cu) catalysts allow focus on the modification of canola fatty acid methyl ester (FAME), a mixture containing 60–70% of oleic, 17–20% of linoleic and 6–10% of linolenic methyl esters [29]. In this way, 5%Ru/HPS catalyst was tested on hydroformylation, the 3%Ru-0.1%Ni/HPS on hydrogenation, the 3%Ru-0.1%Co/HPS on hydroformylation and deoxygenation, and the 3%Ru-0.1%Cu/HPS on oxidative cleavage.

2. Results and Discussion

2.1. Catalyst Characterization

The compiled thermogravimetry for the catalysts 3%Ru/HPS and 3%Ru-0.1%Me/HPS; Me = Co, Ni and Cu is presented in Figure 1. The first weight loss between 35–105 °C is attributed to water chemically and physically adsorbed on the catalyst's surfaces. The second weight loss between 400–500 °C is attributed to the decomposition of the polymeric matrix. However, on every sample, it was possible to verify a subtle onset of weight loss from 250 °C and, therefore, this temperature was chosen as the limit temperature for the catalytic tests.

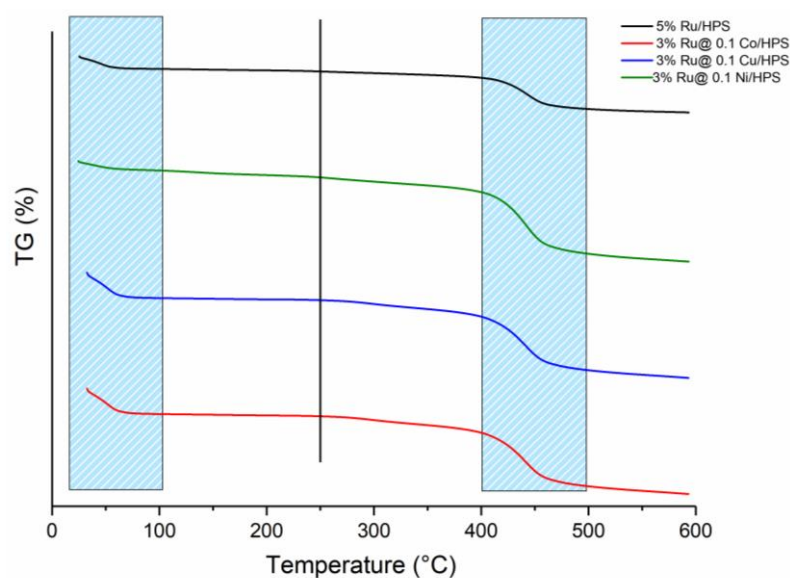


Figure 1. Ruthenium and doped ruthenium/HPS catalysts thermogravimetric profiles.

The catalysts' FT-IR spectrums are compiled in Figure 2. It is possible to verify a similar profile for every sample, with bands between $3100\text{--}2900\text{ cm}^{-1}$ and $1600\text{--}1400\text{ cm}^{-1}$ typical of bond stretching for sp^3 C-H and C-C, as well as vibration and folding for C-H bonds, all of which are associated with the polymeric matrix of HPS.

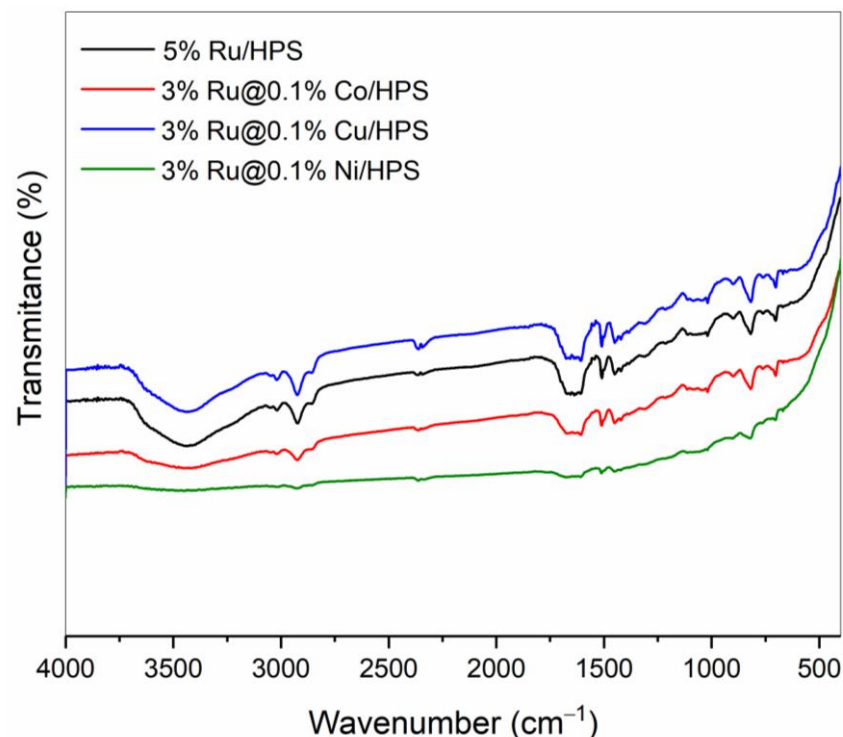


Figure 2. Ruthenium and doped ruthenium/HPS catalysts FT-IR compilation.

To investigate the nature and the amount (mmol g^{-1}) of the acid sites present in these materials, they were analyzed by infrared spectroscopy using pyridine as a probe molecule. Furthermore, the acid strength of the sites was investigated following the thermal stability of the interaction pyridine-acid sites by the acquisition of infrared spectra at 100, 200 and 300 °C [30,31].

The results (Table 1) point out just the presence of a low amount of Lewis acid sites (LAS) in the case of 3%Ru-0.1%Ni/HPS, 3%Ru-0.1%Cu and 3%Ru-0.1%Zn. Bronsted acid sites (BAS) were not detected for any catalysts and no LAS were observed for 3%Ru/HPS and 3%Ru-0.1%Co/HPS; however, it is not possible to ignore the presence of this type of site in very low amounts as they may not be detectable for the analytical strategy employed. It is important to note that even submitted to 300 °C, the detectable acid sites still remain in the material's structure, showing the temperature resistance of the catalysts.

Table 1. Lewis acid sites (LAS) at different temperatures obtained from the infrared spectra using pyridine adsorbed on catalysts.

T (°C)	5%Ru/HPS	3%Ru-0.1%Co/HPS	3%Ru-0.1%Ni/HPS	3%Ru-0.1%Cu/HPS
25	nd	nd	164.2	258.0
100	nd	nd	78.8	140.4
200	nd	nd	61.4	132.5
300	nd	nd	52.9	127.5

nd = non-detected.

The X-ray diffraction patterns of the materials are presented in Figure 3 and just two diffraction bands at 38.35° and 44.50° are observed which can be associated with planes (010) and (011) of metallic ruthenium [32]. The traces of copper, nickel and cobalt present on doped ruthenium catalysts were not present due to their low abundance over the catalysts' surface and equipment detection limit.

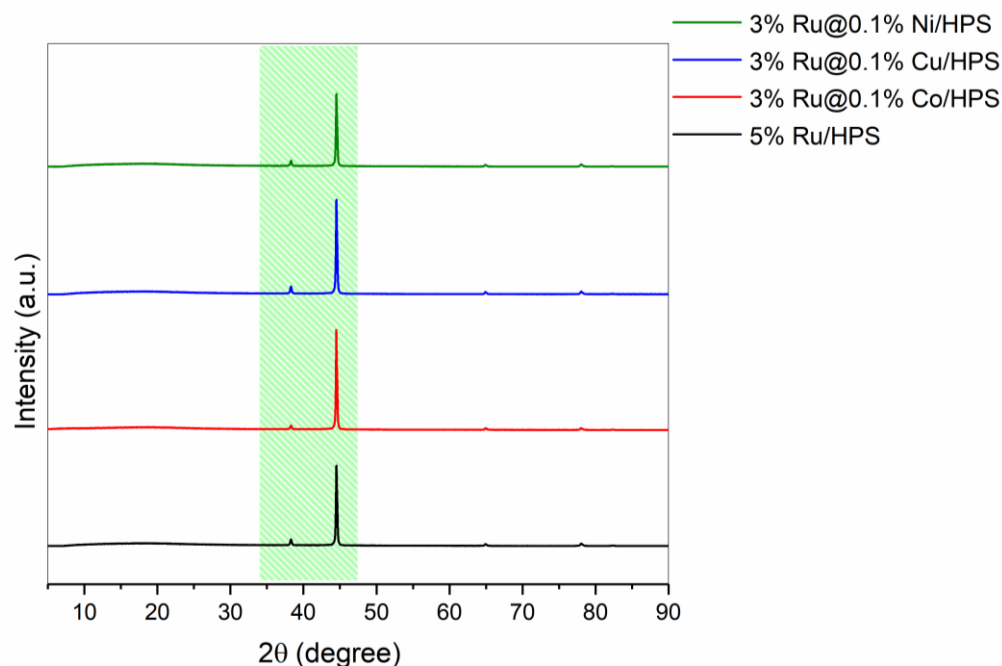


Figure 3. Ruthenium and doped ruthenium/HPS catalysts XRD compilation.

Nitrogen physisorption results for the catalysts (Figure 4 and Table 2) show a slight tendency to decrease on specific surface area and pore volume, in comparison with monometallic 5%Ru/HPS, maybe due to deposition of metallic species in the material walls. All isotherms are of type I, as shown in Figure 4, which are associated with the presence of the hysteresis loop of type H4, indicating mainly the presence of micropores. This observation is confirmed by pore diameter distribution and DBJH values, shown in Figure 5.

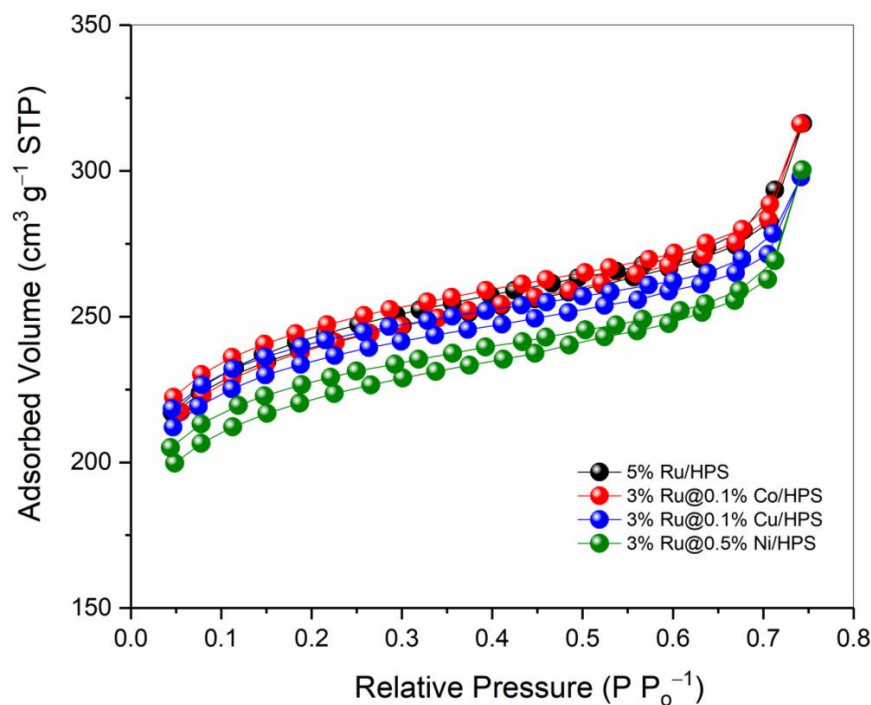


Figure 4. Ruthenium and doped ruthenium/HPS catalysts adsorption–desorption isotherms compilation.

Table 2. BET specific surface area (SBET), pore volume (V) and average pore diameter (DBJH) for doped and non-doped ruthenium/HPS catalysts.

Sample	S _{BET} (m ² g ⁻¹)	V (cm ³ g ⁻¹)	D _{BJH} (Å)
5% Ru/HPS	726	0.125	32.5
3% Ru@0.1% Co/HPS	719	0.121	32.6
3% Ru@0.1% Cu/HPS	712	0.098	36.0
3% Ru@0.1% Ni/HPS	672	0.124	32.4

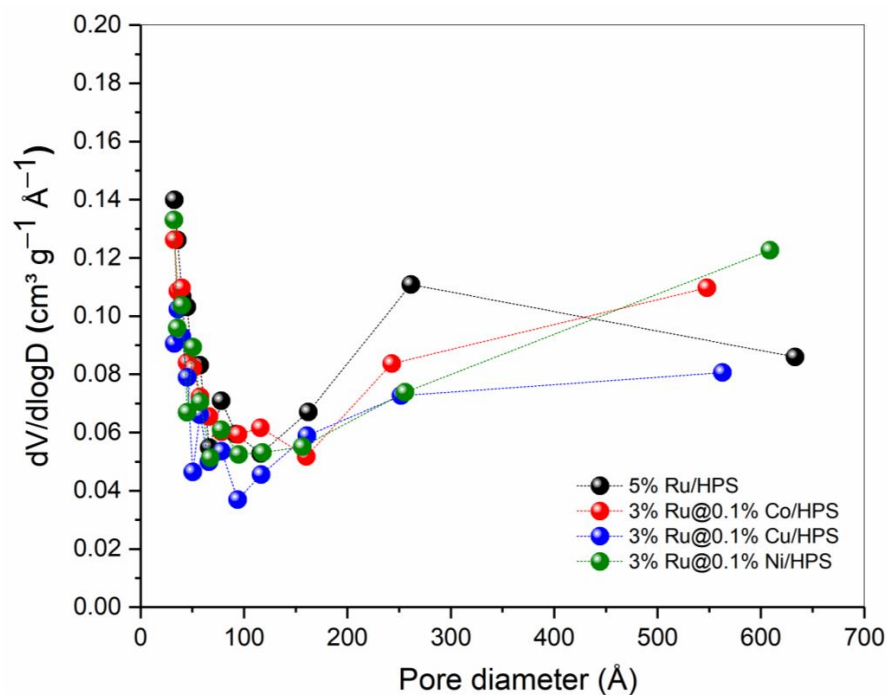


Figure 5. Ruthenium and doped ruthenium/HPS catalysts pore volume distribution compilation.

Previous studies involving 5%Ru/HPS and 3%Ru-0.1%Co/HPS have revealed that for 5%Ru/HPS material hydrated ruthenium (IV) oxide was the predominant form of Ru on the catalyst surface (about 69% of all the ruthenium-containing compounds) and Ru-containing particles are located non-uniformly, mainly closer to the outer surface of the polymer granule. In the case of 3%Ru-0.1%Co/HPS, no products of chemical interaction of cobalt and ruthenium were detected and cobalt is present as $\text{Co}(\text{OH})_2$ [28,33].

The dispersion parameters observed in previous studies were obtained, as shown on the SEM compilation in Figure 6. The introduction of cobalt, nickel and copper changes the distribution of ruthenium-containing particles, increasing their uniformity. Copper promoted the greatest dispersion followed by nickel and cobalt. Other SEM images in different zooms are available in the supporting information, Supplementary Material Figures S1–S16.

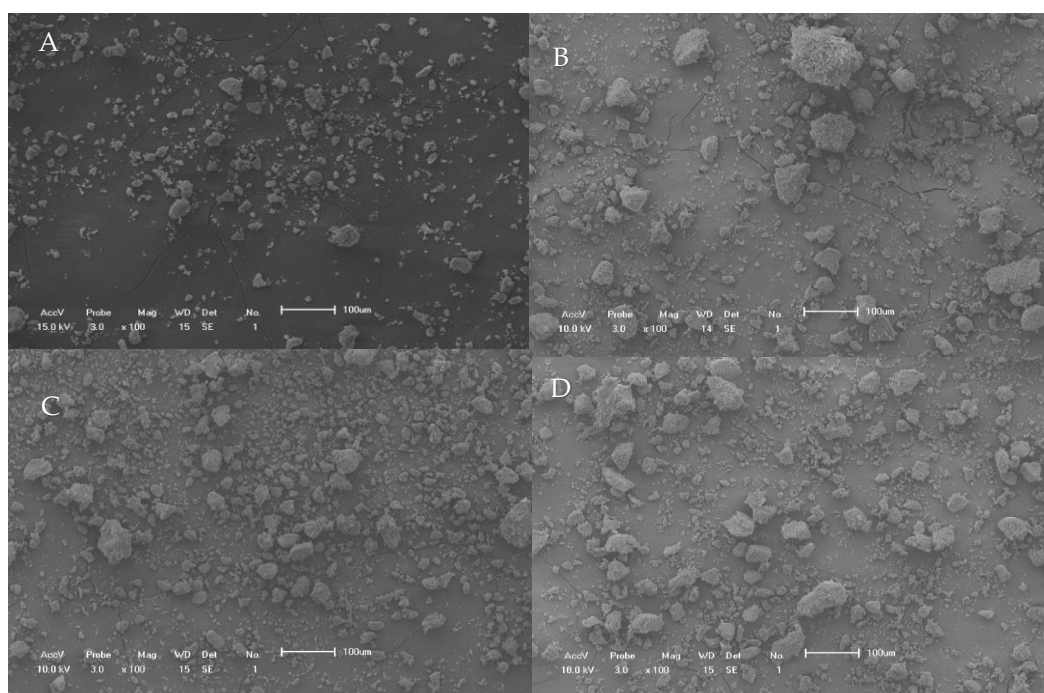


Figure 6. SEM 100 \times magnification compilation. (A) 5%Ru/HPS; (B) 3%Ru@0.1%Co/HPS; (C) 3%Ru@0.1%Cu/HPS e; (D) 3%Ru@0.1%Ni/HPS.

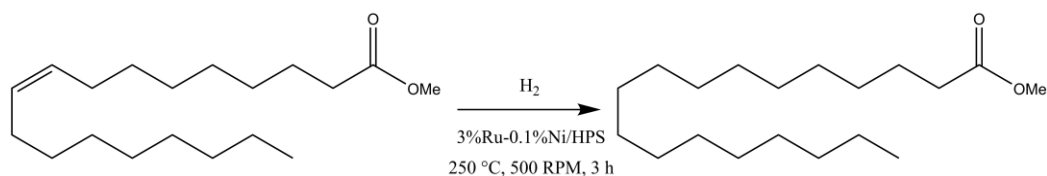
2.2. Catalyst Activity Tests

The canola FAME mixture was chosen as substrate due to its major composition of 70% methyl oleate [29], which is less expensive if compared to pure oleic acid which is obtained by fraction, facilitating the application of this catalytic system on greater scales. The usage of FAME mixtures is therefore friendly to circular economic applications while contributing to green chemistry, enhancing the sustainability of a process. On the other hand, the methyl oleate has also only one unsaturation per fatty chain which facilitates the interpretation of activity data [4,34,35].

The FT-IR of both canola oil and canola FAME shows only the shifting of carbonyl stretch from 1743 cm^{-1} on oil to 1743 cm^{-1} on FAME, as demonstrated in Supplementary Material Figure S17. The ^1H NMR for the canola FAME (Supplementary Material Figure S18) demonstrates the disappearance of internal hydrogens of glycerol over 4.40 and 4.15 ppm, while also showing the appearance of a methyl peak at 3.67 ppm, indicating almost total conversion of oil into FAME. The GC-MS chromatogram of canola FAME and main component list are also available in Supplementary Material Figure S19 and Table S1.

The hydrogenation methodology chosen, Scheme 2, was typical of heterogenized nickel catalytic systems. On the heating ramp, over $175\text{ }^\circ\text{C}$, it was possible to verify a

10 bar fall, indicative of activity at temperatures lower than the selected and also effectivity at the oxidative addition step, considered the limiting catalytic step for hydrogenations. The obtained white and solid product was extracted with petroleum ether to avoid HPS solubilization [36].



Scheme 2. Hydrogenation of canola FAME.

The hydrogenation of canola FAME with 3%Ru@0.1%Ni/HPS showed an outstanding result with the apparent total conversion of starting unsaturations, using 50 bar of H₂, at 250 °C and 500 rpm, during 180 min. The FT-IR spectrum of the hydrogenated canola FAME product, Figure 7, shows the disappearance of the C-H sp² stretch band, while the ¹H NMR spectrum, Figure 8, allows the conversion calculation at 99%. The calculation of selectivity and yield was not possible due to the superposition of fatty chain hydrogens. The GC-MS chromatogram and main component list, Supplementary Material Figure S20 and Table S2, corroborate the full conversion of canola FAME into saturated fatty chains. The high activity justification is due to synergic effects between nickel and ruthenium allowing a greater dispersion of particles over the catalyst surface, as shown on the SEM and greater acid stability at high temperatures if compared to 5%Ru/HPS.

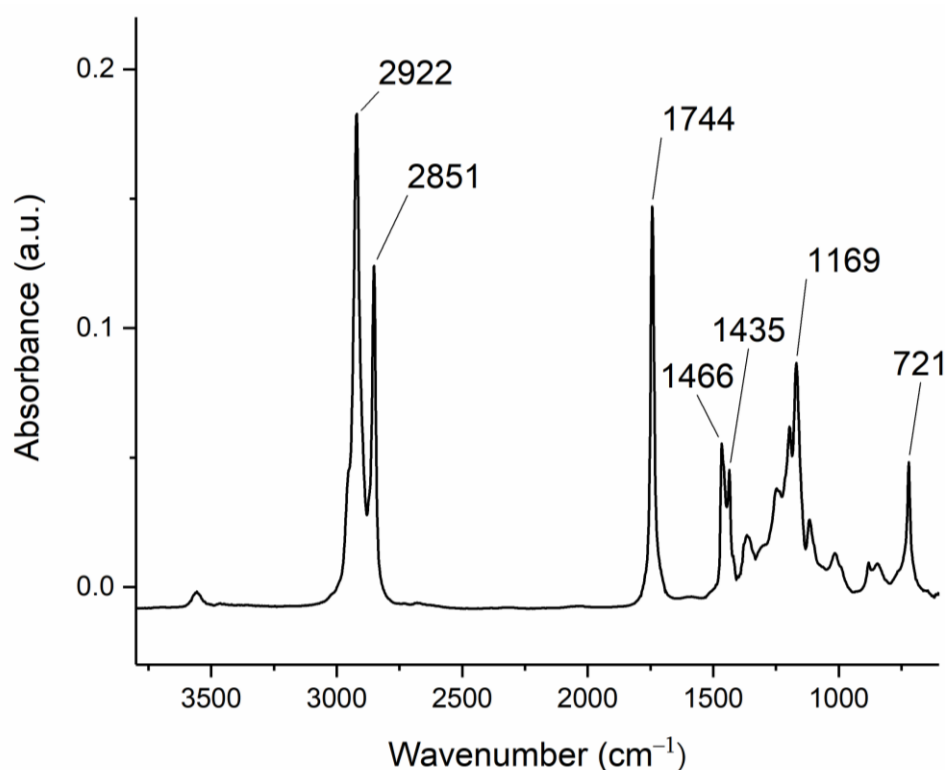


Figure 7. FT-IR spectrum for hydrogenated canola FAME.

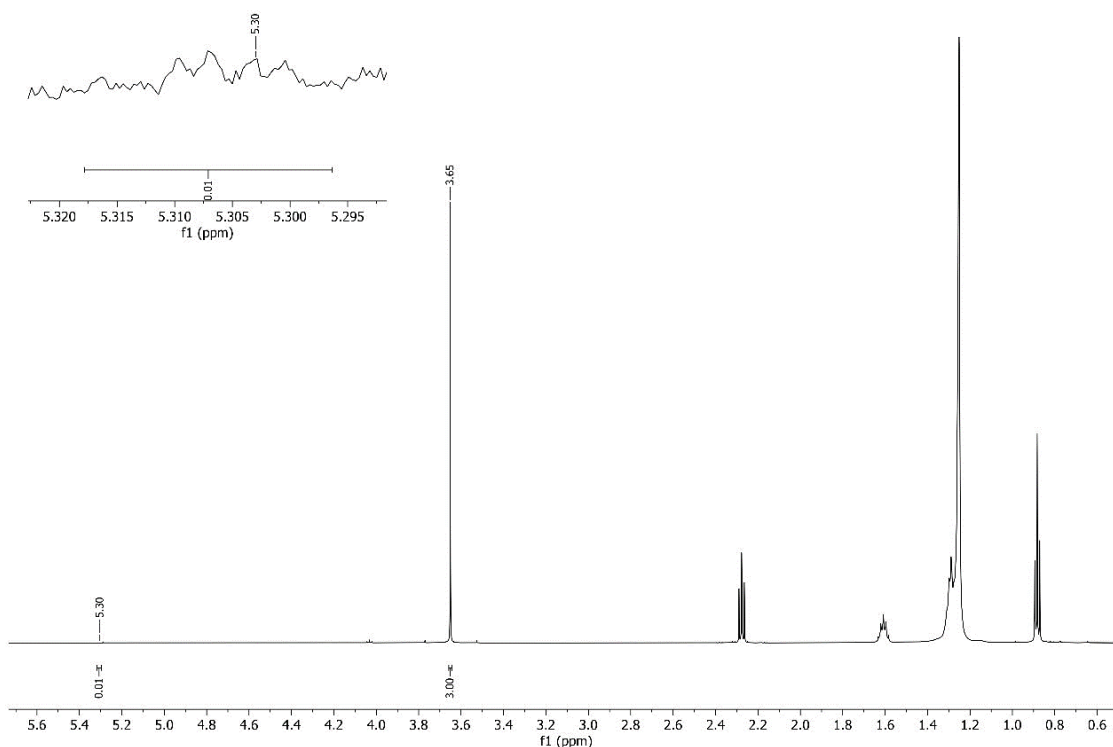


Figure 8. ^1H NMR spectrum for hydrogenated canola FAME.

An example from the literature points out that ruthenium supported over carbon was studied on hydrogenation of soybean oil (2 bar of H_2 at $165\text{ }^\circ\text{C}$) resulting in moderate non-selective yields (18.8% of linoleic (C18:2), 53.3% of oleic (C18:1) and 14.4% of stearic (C18:0) fatty chains) [37]. In another study, the hydrogenation of glycerol trioleate (1.60 mmol of the double bond) was described in the presence of ruthenium nanoparticles supported over ion exchange resin DOWEX-300 using water:heptane at $30\text{ }^\circ\text{C}$, 10 bar of H_2 and 1000 rpm, during 120 min, yielding 45% of unsaturations conversion [38]. Nanocatalysts containing nickel, palladium and ruthenium were also applied on the selective hydrogenation of canola oil attaining 75.3% of cis-C18:1 and 2.46% of C18:0, at $100\text{ }^\circ\text{C}$, 10 bar of H_2 and 500 rpm, during 60 min [39].

The first hydroformylation followed a classical heterogenized ruthenium methodology with syn-gas (1:1), toluene and 5%Ru/HPS as catalyst, under $150\text{ }^\circ\text{C}$ for 48 h. In contrast with the hydrogenation, no pressure fall was detected, indicating no intense activity. The obtained product ^1H NMR (Figure 9) allows the calculations of conversion and selectivity for aldehyde and yield, 44.23%, 1.8% and 0.8% respectively. As there were no signs of alcohol, most of the conversions were into hydrogenated products, while the mild temperature of $150\text{ }^\circ\text{C}$ might not be enough for the oxidative addition step, stimulating the selection of another methodology.

The second hydroformylation test, Scheme 3, followed a slightly more drastic methodology with syn-gas (1:1), no solvent, 3%Ru@0.1%Co/HPS as catalyst, under $250\text{ }^\circ\text{C}$ for 4 h. The cobalt-doped ruthenium catalyst was chosen due to the famous cobalt synergic effect over ruthenium aiming for higher activities. Indeed, as expected, a pressure fall was verified and the obtained product was partially solidified.

The hydroformylated canola FAME FT-IR spectrum, Figure 10, shows intensity reduction on the C-H sp^2 stretch band, while the ^1H NMR spectrum, Figure 11, allows the conversion calculation at 89%, but with no signals of aldehyde or alcohol, indicating the materials hydrogenation. The calculation of selectivity and yield was not possible due to the superposition of fatty chain hydrogens. The GC-MS chromatogram and main component list, Supplementary Material Figure S21 and Table S3, corroborate the conversion of canola FAME into saturated fatty chains. In comparison with the nickel-doped ruthenium/HPS,

the lower activity was either due to the addition of carbon monoxide or to the catalyst acid properties, lower than the nickel-doped.

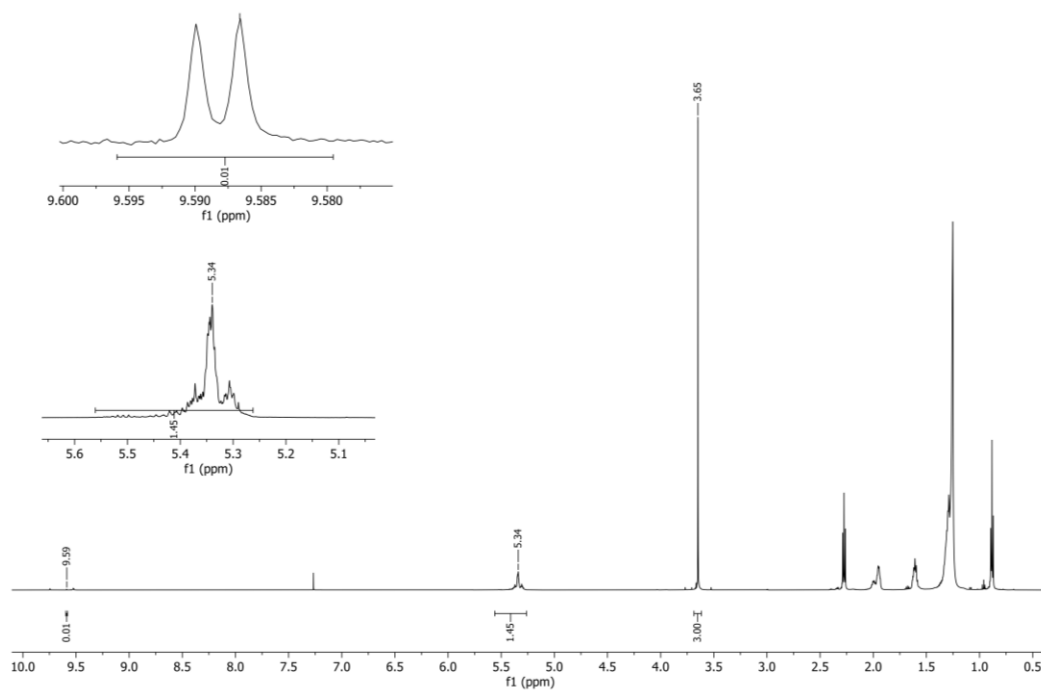
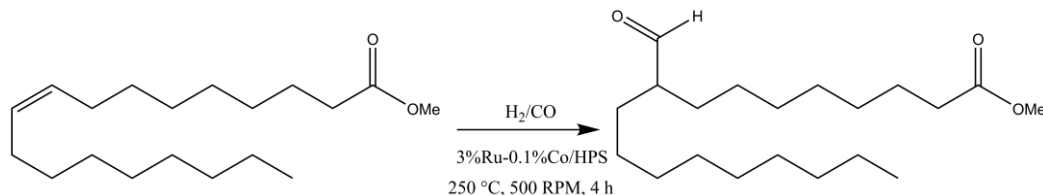


Figure 9. ^1H NMR spectrum for hydroformylated product following the first methodology.



Scheme 3. Hydroformylation methodology was chosen for the canola FAME modification.

The canola FAME oxidative cleavage methodology, Scheme 4, was adapted from classical heterogenized ruthenium on the oxidation of unsaturations, with sodium periodate as co-oxidant, 3%Ru@0.1Cu/HPS as catalyst and a solvent mixture in a glass flask at room temperature during 48 h. The oxidative cleavage was simpler in comparison with the hydrogenations, requiring no gas pressure and no product extraction. The copper-doped ruthenium catalyst was chosen due to its promoter properties on oxidative cleavage reactions. The oxidized canola FAME FT-IR spectrum, Figure 12, show the total disappearance of the C-H sp^2 band stretch and asymmetry on the carbonyl C=O stretch band indicating the formation of other carbonylated species.

The ^1H NMR spectrum for the oxidized canola FAME, Figure 13, allows the conversion of 85%. Values for selectivity and yield were not calculated due to the hydrogen labile character on the oxidized major products azelaic acid and pelargonic acid, while the ester variations of such overlap with the starter fatty chain hydrogens. The ^1H NMR allowed the identification of an aldehyde triplet at 9.7 ppm, coupled with hydrogens β to the carbonyl position, with calculated selectivity for aldehyde calculated at 17%. The aldehyde presence is explained by a possible water addition during the oxidative cleavage process. The ^{13}C NMR, Figure 14, shows the characteristic peaks of aldehyde at 200 ppm, carboxylic acid at 180 ppm, ester at 172 ppm and unsaturation at 130 ppm, indicating the partial conversion. The corroborative GC-MS chromatogram and main component list are available in Supplementary Material Figure S22 and Table S4. Among the tested catalysts,

the copper-doped ruthenium/HPS was the most acidic and presented the greater pore volume and greater dispersion on the support surface and these characteristics explain the elevated activity at room temperature.

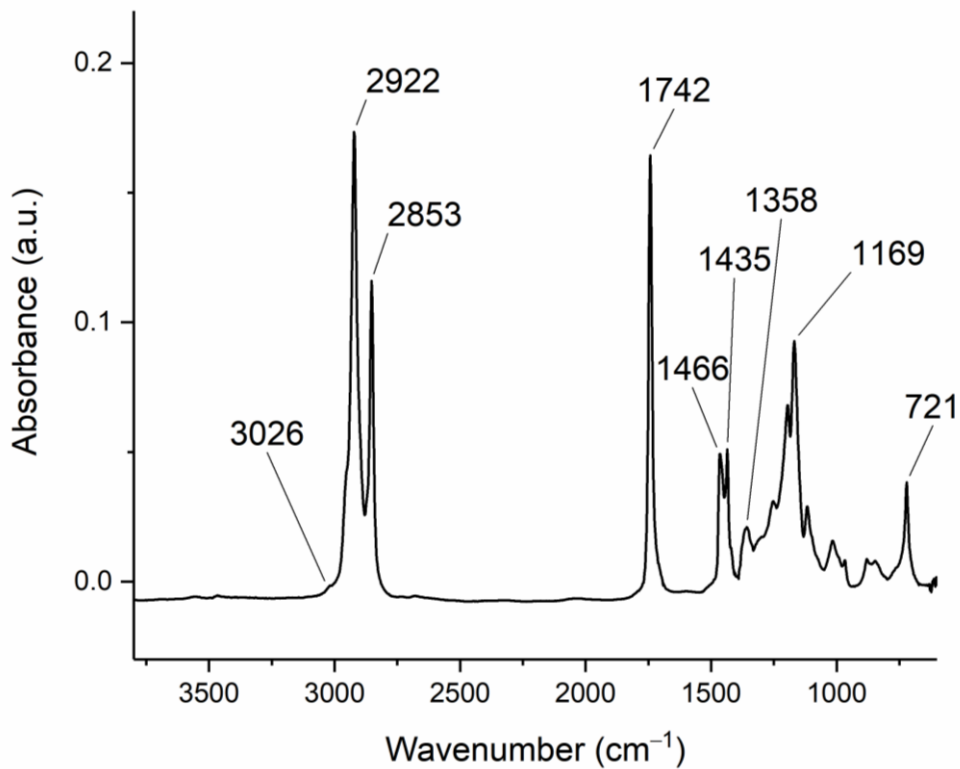


Figure 10. FT-IR spectrum for hydroformylated canola FAME product on the second methodology.

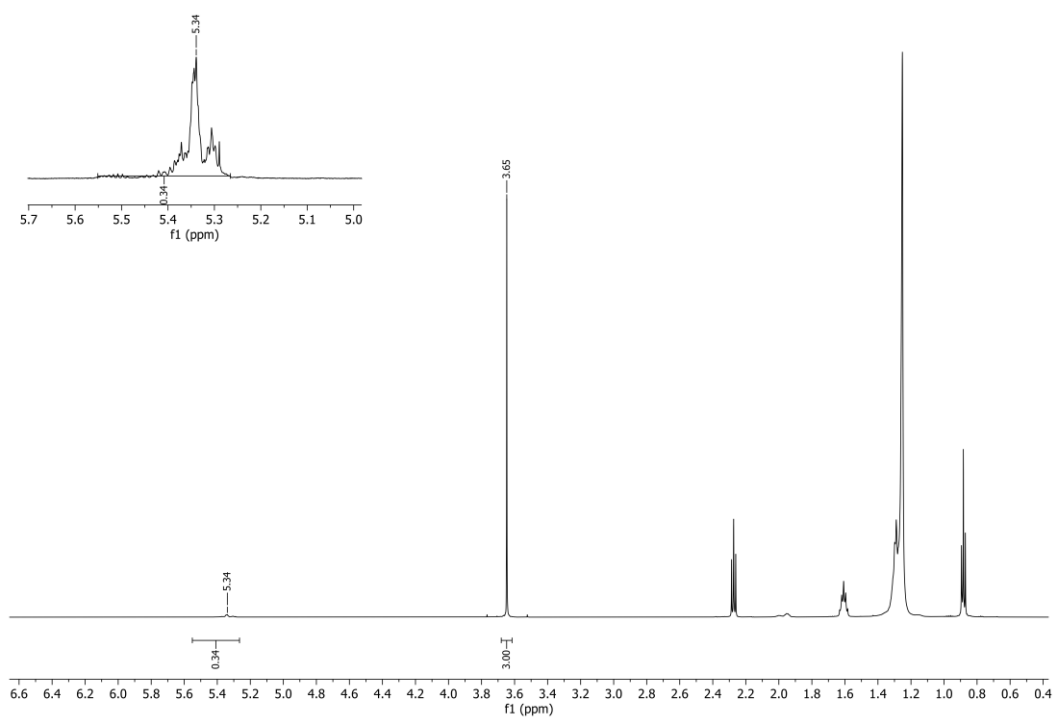
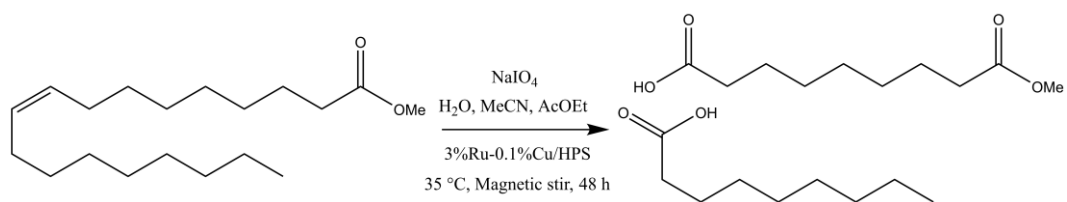


Figure 11. ¹H NMR spectrum for hydroformylated canola FAME product on the second methodology.



Scheme 4. Oxidative cleavage of canola FAME.

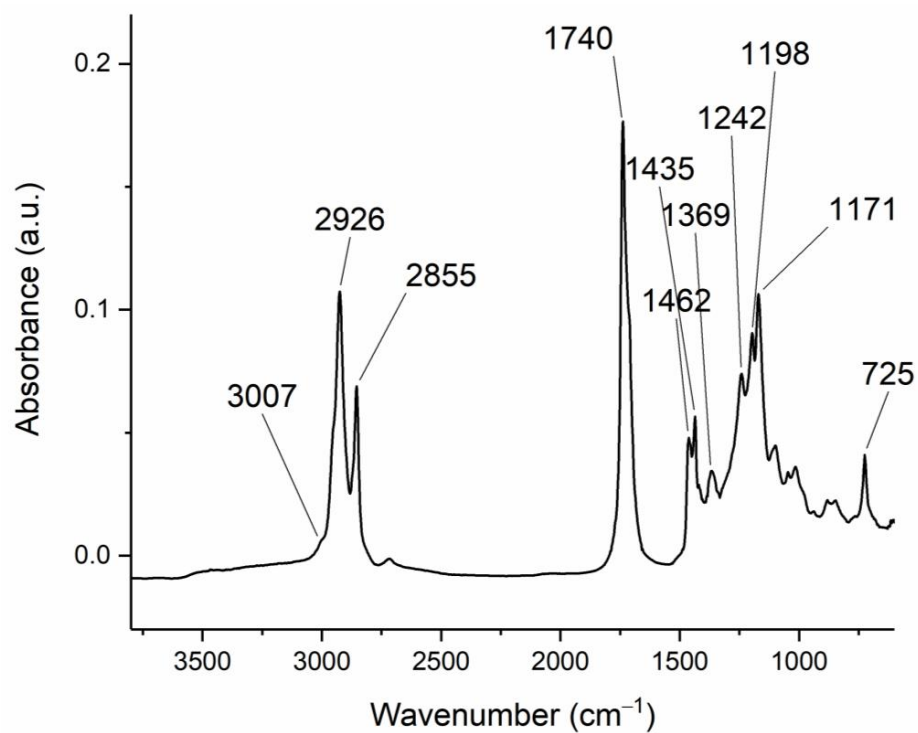


Figure 12. FT-IR spectrum for oxidized canola FAME product.

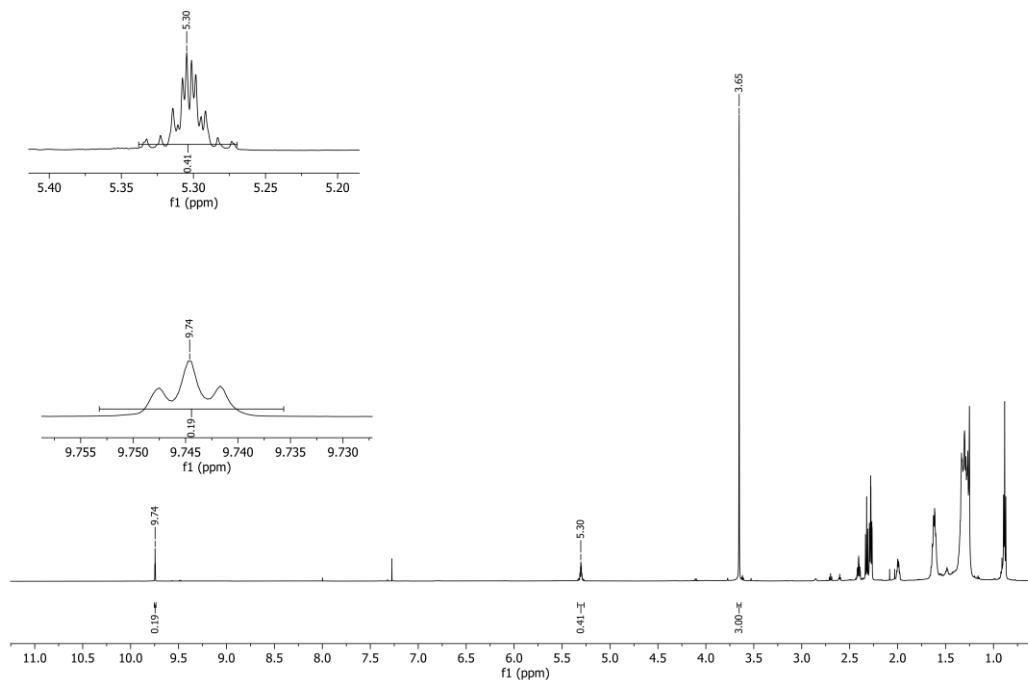


Figure 13. ¹H NMR spectrum for oxidized canola FAME product.

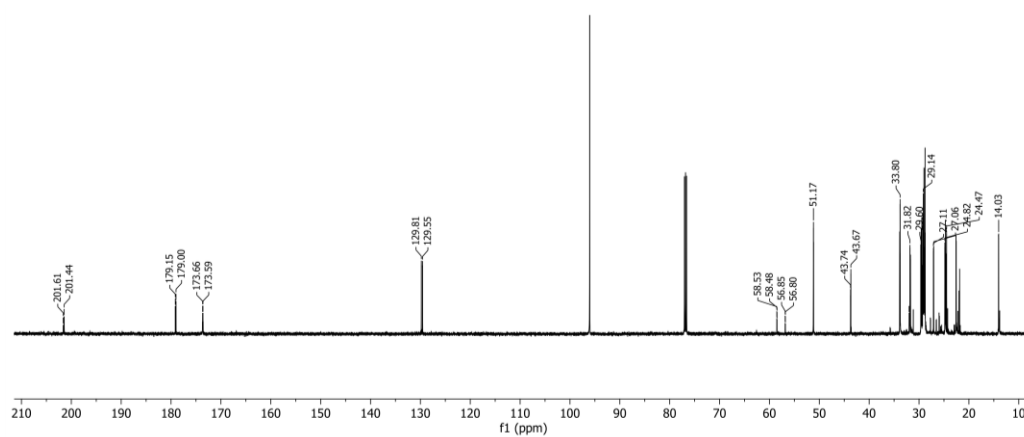
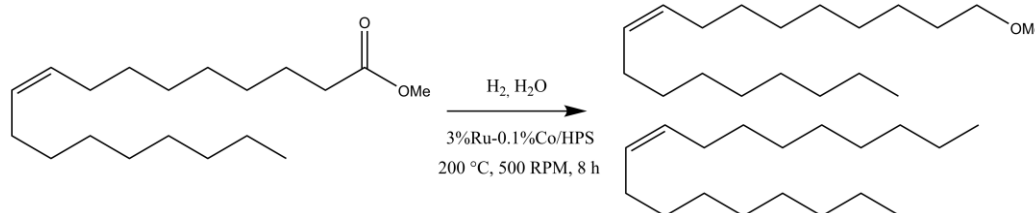


Figure 14. ^{13}C NMR spectrum for oxidized canola FAME product.

Few examples of oxidative cleavage of fatty compounds using supported ruthenium catalysts are available in the literature. A catalytic system based on ruthenium nanoparticles supported on hydroxyapatite was used for the oxidative cleavage of oleic acid and 16% of unsaturation conversion and 84% of pelargonic acid yield were detected, after 12 h at room temperature [40]. In another study, a functionalized carbon black support for the complexation of ruthenium was tested on oxidative cleavage of oleic acid, yielding almost complete conversions to pelargonic and azelaic acids, after 24 h and 1500 rpm at room temperature [41].

The deoxygenation methodology of canola FAME with 3%Ru@0.1%Co/HPS, Scheme 5, was the same as for hydrogenation, but using milder conditions (30 bar of H_2 , 200 °C and 500 rpm), in the presence of water and longer reaction time. The cobalt-doped ruthenium/HPS catalyst was selected due to the cobalt synergic properties over the ruthenium clusters. The obtained product was a white solid associated with the occurrence of hydrogenation and decarbonylation. The FT-IR of the product, Figure 15, shows the total disappearance of the C-H sp^2 band stretch and decreased carbonyl C=O stretch band, indicating the formation of hydrogenated and decarbonylated species.



Scheme 5. Deoxygenation of canola FAME.

The ^1H NMR for the deoxygenated product, Figure 16, shows almost the total disappearance of unsaturation and methoxyl peaks. The conversion calculations were possible by normalization based on the chain methyl group, at 0.88 ppm, which was similarly done to the starter FAME ^1H NMR. The calculated conversions for unsaturation and methoxyl were 99%. On the ^{13}C NMR, Figure 17, is possible to verify the total disappearance of unsaturations peaks and the presence, although at a very low intensity, of ester at 173 ppm, carboxylic acid at 179 ppm and ether terminal carbon at 64 ppm. The corroborative GC-MS chromatogram and main component list are available in Supplementary Material Figure S23 and Table S5.

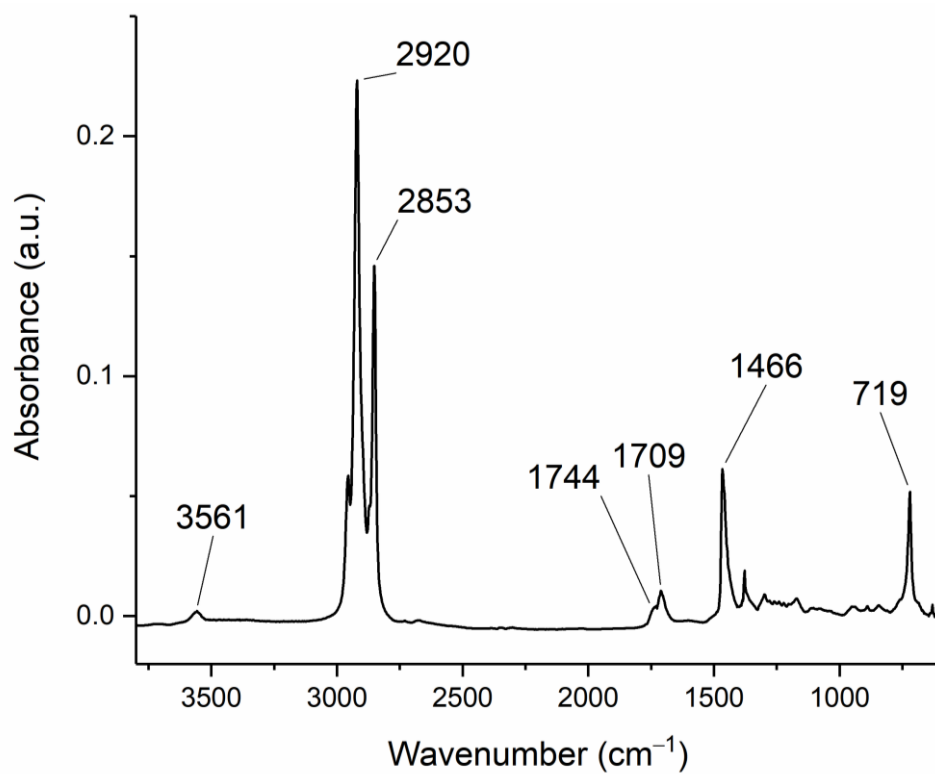


Figure 15. FT-IR spectrum for deoxygenated canola FAME product.

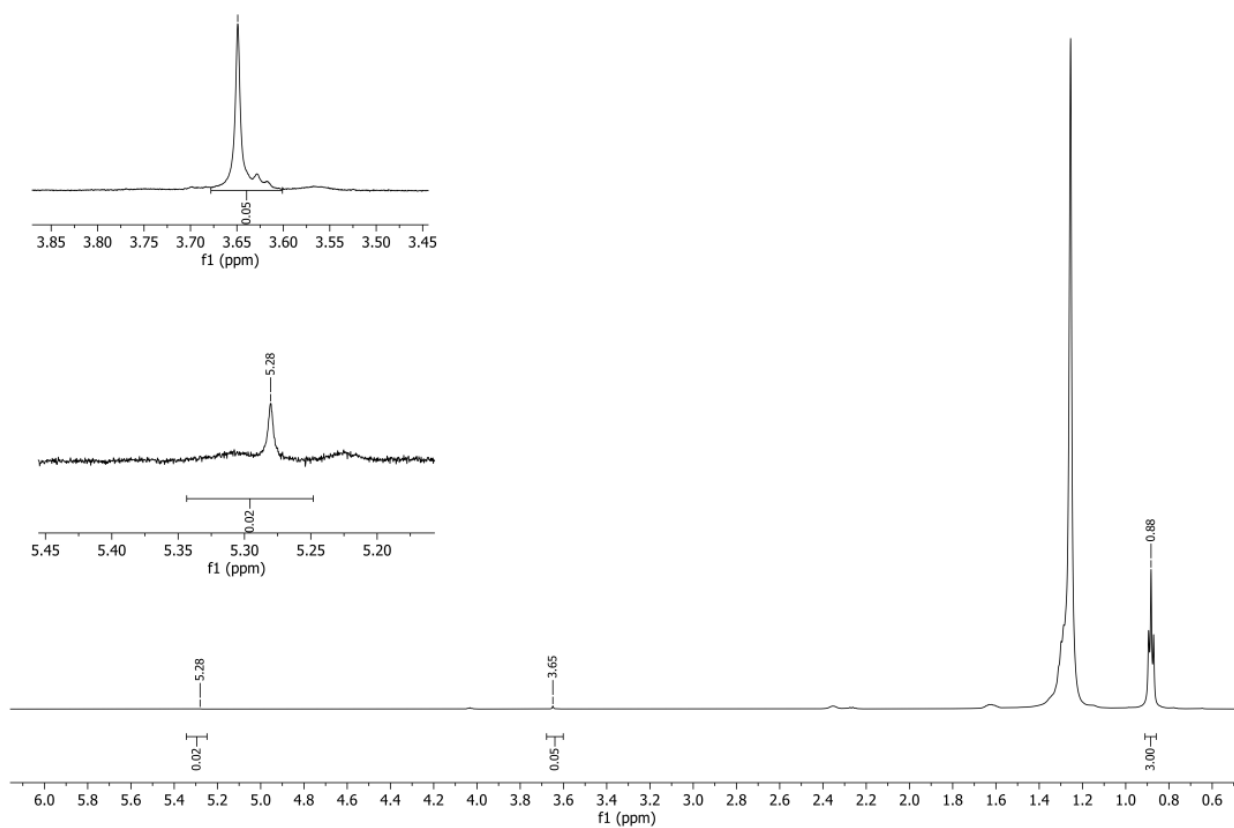


Figure 16. ^1H NMR spectrum for deoxygenated canola FAME product.

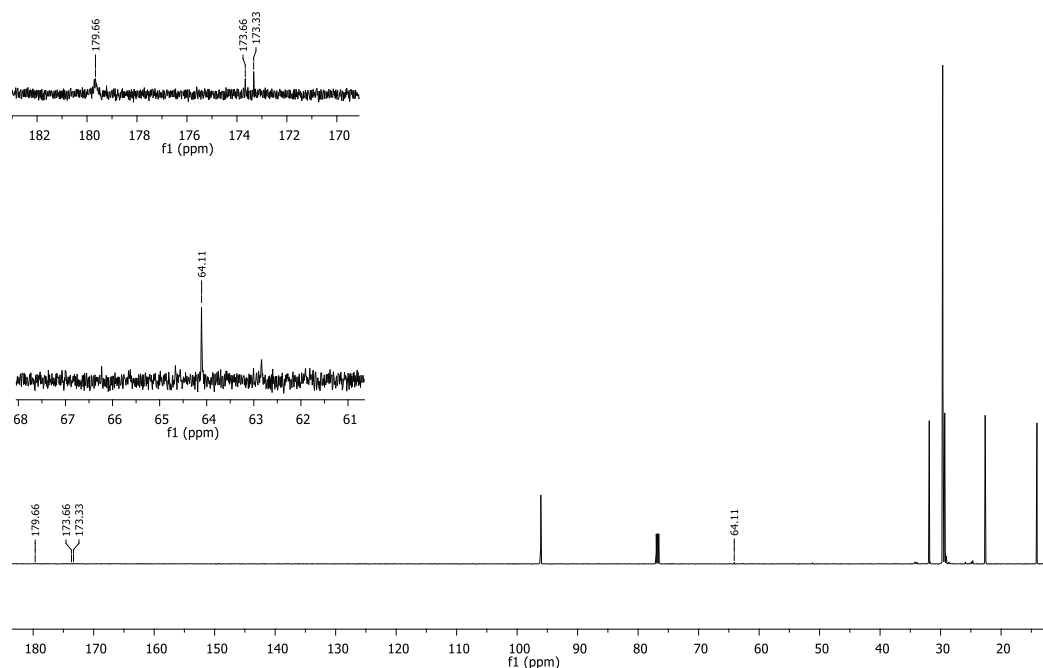


Figure 17. ^{13}C NMR spectrum for deoxygenated canola FAME product.

It is important to mention some examples from the literature. Stearic acid was deoxygenated using hexane, 68 bar of H_2 and 50 mg of 10%Co/HPS, at 250 °C for 1 h with total conversion [42]. The deoxygenation of waste cooking oil using water and ruthenium supported over hydroxyapatite catalyst was studied. In this case, conversions over 100% and an yield of 89% of alkane long chain were attained at 180 °C, 20 bar of H_2 and 1000 rpm, for 4.5 h. Additionally, the catalyst could be recycled [43]. Deoxygenation of tall oil fatty acids was tested using carbon-supported ruthenium nanoparticles in the presence of aqueous formic acid at 326 °C and 2 h, leading to high conversion (~100%) and selectivity of the 82% to C5–C20 alkane chains [44]. Ruthenium nanoparticles on a porous organic network were employed on the deoxygenation of stearic acid (30 bar of H_2 , 180 °C, 8 h) with high conversion and selectivity [45]. However, herein, using canola FAME, a not hydrogenated substrate, was possible to hydrogenate and deoxygenate under milder conditions of pressure and temperature, and with fewer metallic sites, all indications of great catalyst activity.

In summary, the applications tested and discussed here, many of them with extremely promising results, demonstrated the potential of catalysts based on ruthenium heterogenized species. From these encouraging results, subsequent optimization works can be carried out, in which distinct catalysts and residual fatty substrates can be studied at several reaction conditions.

3. Materials and Methods

3.1. Materials

The reagents used for the catalyst preparation and characterization were analytical grade and used as received. The canola oil, used for canola FAME synthesis, was food-grade and used as received.

3.2. Catalyst Synthesis

The doped and non-doped ruthenium/HPS catalysts were prepared by wet impregnation methodologies described elsewhere [26,28,33,42]. The simpler non-doped ruthenium catalyst (5%Ru/HPS) was prepared by a wash of the hypercrossed polystyrene (3 g) with water and acetone, followed by impregnation of $\text{Ru}(\text{OH})\text{Cl}_3$ (on adequate molarity considering wt% of metal) dissolved in tetrahydrofuran, methanol and water (5:1:1). After the

impregnation, the mixture was dried at 70 °C for 1 h, refluxed with 21 mL of a 0.1 mol L⁻¹ NaOH solution and strongly agitated with 2 mL of hydrogen peroxide. The impregnated catalyst was washed, dried and reduced with a H₂ flux of 100 mL min⁻¹ at 300 °C for 2 h.

Similarly, on the doped ruthenium/HPS (3%Ru-0.1%Me/HPS, Me = Co, Ni and Cu), the appropriate molarities of acetates of cobalt(II), copper(II) and nickel(II) were dissolved with the Ru(OH)Cl₃ on the mixture of tetrahydrofuran, methanol and water. The materials were analyzed without previous treatment by the technique described below.

3.3. Catalyst Characterization

Thermogravimetric characterizations were performed using a Shimadzu TGA-50 apparatus under a nitrogen atmosphere in the temperature range from 25 to 1000 °C, at a heating rate of 10 °C/min.

The FTIR spectra were recorded on a Shimadzu IR Prestige 21 spectrometer using the KBr pellet method. The following operational parameters were used: spectral range of 400–4000 cm⁻¹, 65 scans in transmittance mode and a resolution of 4 cm⁻¹. For pyridine (Py)-adsorption infrared spectroscopy tests, a KBr pellet (sample and KBr were weighed) was placed in a closed receptacle containing liquid pyridine (none in direct contact with the pellet) and a vacuum was formed to obtain pyridine vapor. The system remained under this condition for 48 h so that pyridine vapor could interact with the acid sites of the samples. After this procedure, the infrared spectra were acquired at 25 °C and after an increase in temperature of 100, 200 and 300 °C.

In all cases, the number of acid sites was evaluated by integrating the area of the absorption bands related to different acid sites (Bronsted or Lewis) using Equation (1), in which D = pellet diameter (cm), w = mass of the sample (g), and $A_{B,L}$ = integration of the Lewis and Bronsted characteristic bands: approximately 1537 cm⁻¹ for Py-Bronsted site and 1445 cm⁻¹ (Py-Lewis site). The coefficient of extinctions of the Py-Bronsted interaction site and of the Py-Lewis site are 1.67 ± 0.12 cm μmol⁻¹ and 2.22 ± 0.21 cm mol⁻¹, respectively.

$$q_{B,L} = (A_{B,L} \cdot \pi \cdot D^2) (4w \cdot E_{B,L}) \quad (1)$$

X-ray diffraction (DRX) measurements on powder samples, were performed on a Rigaku Multiflex instrument equipped with nickel filtered Cu K (0.15418 nm) radiation source and a scintillation counter detector. The data were selected in the range of 2θ from 2 to 80 ° at a goniometer speed of 2°/min and a step of 0.02 ° with a counting time of 1 s at each step. The crystallite sizes were determined by the Scherrer equation (Equation (2)).

$$D_{hkl} = \frac{K\lambda}{\beta \cos(\theta)} \quad (2)$$

The nitrogen physisorption isotherms at 77 K were obtained using a Quantachrome Nova 2200e Instrument. The specific surface area was determined by the Brunauer–Emmett–Teller method.

Microscopy images of the samples were obtained using a Hitachi scanning electron microscope (SEM), model S-3400N (all the samples were previously metalized with gold), and an FEI Tecnai G2 Spirit TWIN transmission electron microscope (TEM) (120 kV).

3.4. FAME Synthesis and Activity Tests

This canola FAME mixture was obtained by alkaline transesterification of canola oil following established methodologies [46]. The activity tests for 3%Ru-0.1%Me/HPS, Me = Co, Ni and Cu consisted of modifications of FAME by hydrogenation, hydroformylation, oxidative cleavage and deoxygenation. The obtained products were analyzed by FT-IR and ¹H/¹³C NMR.

The hydrogenation methodology was adapted from the literature [47], using a 100 mL Parr reactor model 4590 HP. Before usage, the Parr reactor was meticulously cleaned with steel wool and tuned for each mixture's temperature without the catalysts (canola

FAME and hydrogen, canola FAME water and hydrogen, etc.), and no pressure fall was observed. To the reactor were added 10 mL of dry canola FAME and 200 mg of catalyst (3%Ru-0.1%Ni/HPS). The reactor was purged and pressurized to 20 bar of N₂. After the pressurization, the system was almost totally depressurized and pressurized with H₂ to 50 bar. The pressurized system was heated to 250 °C and stirred under 500 RPM for 3 h. Past the reaction time, the system was cooled, quenched by depressurization, the obtained mixture dissolved in petroleum ether, filtered in alumina and the product dried under reduced pressure.

For the hydroformylation, two adapted methodologies were applied. First, [48–50], to a 150 mL autoclave reactor, with glass cup and magnetic stirring, was added 1.76 mL of dry canola FAME, 168 mg of catalyst (5%Ru/HPS) and 5 mL of dry toluene. The reactor was purged and pressurized to 20 bar of N₂. After the pressurization, the system was almost totally depressurized and pressurized with CO to 25 bar and H₂ to 50 bar. The pressurized system was heated to 150 °C and magnetically stirred for 48 h. Past the reaction time, the system was cooled, quenched by depressurization, the obtained mixture dissolved in toluene, filtered in alumina and the product dried under reduced pressure.

Second, hydroformylation methodology was applied, adapted from literature [47], using a 100 mL Parr reactor model 4590 HP. To the reactor was added 10 mL of dry canola FAME and 140 mg of catalyst (3%Ru-0.1%Co/HPS). The reactor was purged and pressurized to 20 bar of N₂. After the pressurization, the system was almost totally depressurized and pressurized with CO to 25 bar and H₂ to 50 bar. The pressurized system was heated to 250 °C and stirred under 500 RPM for 4 h. After the reaction time, the system was cooled, quenched by depressurization, the obtained mixture dissolved in petroleum ether, filtered in alumina and the product dried under reduced pressure.

The oxidative cleavage methodology was adapted from applications for ruthenium complexes methodologies found elsewhere [51]. To a glass flask was added 4 mL of canola FAME, 12 g of sodium periodate, 30 mL of distilled water, 20 mL of acetonitrile, 20 mL of ethyl acetate and 78 mg of catalyst (3%Ru-0.1%Cu/HPS). The mixture was magnetically stirred at room temperature for 48 h. After the reaction time, the products were extracted with petroleum ether, filtered in alumina and dried under reduced pressure.

The deoxygenation methodology was adapted from the literature [52,53] for a 100 mL Parr reactor model 4590 HP. To the reactor was added 0.7 mL of canola FAME, 10 mL of mili-Q water and 150 mg of catalyst (3%Ru-0.1%Co/HPS). The reactor was purged and pressurized to 20 bar of N₂. After the pressurization, the system was almost totally depressurized and pressurized with H₂ to 30 bar. The pressurized system was heated to 200 °C and stirred under 500 RPM for 8 h. After the reaction time, the system was cooled, quenched by depressurization, the obtained mixture dissolved in petroleum ether, filtered in alumina and the product dried under reduced pressure.

The FT-IR were recorded using a Shimadzu IR Prestige 21 spectrometer with an ATR Miracle cell. The following operational parameters were used: spectral range of 650–4000 cm⁻¹, 32 scans in absorbance mode and a resolution of 4 cm⁻¹. The ¹H/ ¹³C NMR spectra were obtained from a Bruker 600 MHz NMR spectrometer, equipped with a broad-band probe Bruker 5 mm (BBFO). Spectrums were obtained for ¹H and ¹³C on deuterated chloroform, referenced with TMS, using 16 scans for ¹H and 2000 scans for ¹³C and 5 s delay.

The GC-MS chromatograms were obtained using a Shimadzu GC-MS model QP-2020. The samples were eluded through a Zebron Phase 0.5 µm thickness × 0.25 mm diameter × 50 m length. Samples were diluted in hexane (1:10). The column initial temperature was 60 °C, which was maintained for 5 min, and then ramped from 60 °C to 270 °C at 2 °C min⁻¹. At 270 °C, the temperature was maintained for 5 min. The injection temperature was 280 °C, the ion source temperature was 200 °C and the interface temperature was 280 °C. The injected volume was 1 µL with a split of 1:100. The helium analytical grade was used on a flow rate of 0.95 mL min⁻¹.

The activity quantification method was found in the literature, using the integrated areas from ^1H NMR [54,55]. The Double Bond Number (DBN) was determined using Equation (3), where B is the unsaturation area over 5.3 ppm and A is the methyl group over 3.6 ppm. The variation of DBN before and after is possible to determine the conversion, as stated in Equation (4).

$$\text{DBN} = \frac{\frac{B}{2}}{\frac{A}{3}} \quad (3)$$

$$\text{Conversion}(\%) = \frac{\text{DBN}_i - \text{DBN}_f}{\text{DBN}_i} \times 100 \quad (4)$$

The selectivity values for the hydroformylated samples were calculated using Equation (5), where C is the aldehyde hydrogen duplet over 7.1 ppm and A is the methyl group over 3.6 ppm. The yield values for hydroformylated samples were determined using Equation (6).

$$\text{Aldehyde selectivity}(\%) = \frac{\frac{C}{3}}{\text{DBN}_i - \text{DBN}_f} \times 100 \quad (5)$$

$$\text{Yield}(\%) = \frac{\text{Conversion} \times \text{Selectivity}}{100} \quad (6)$$

4. Conclusions

Different catalysts based on ruthenium and doped ruthenium supported on the surface of hypercrosslinked polystyrene were prepared by wet impregnation. The catalysts were characterized for acidity, morphology, surface area and thermic stability to select possible applications. Canola FAME was chosen as the substrate due to its major composition of oleic acid. The catalysts were highly active for hydrogenation, with a conversion of 99%, and effective on oxidative cleavage reactions, with a conversion of 85%. The catalyst was also extremely active for deoxygenation reactions, on which double behavior was observed, simultaneously deoxidizing and hydrogenating the canola FAME with conversions of 99%. The obtained data stimulates further collaborative studies for optimization using distinct catalysts and residual fatty substrates at several reaction conditions.

Supplementary Materials: The following supporting information can be downloaded at: <https://www.mdpi.com/article/10.3390/catal13030630/s1>, Figure S1. 5%Ru/HPS 100× magnification SEM; Figure S2. 5%Ru/HPS 3000× magnification SEM; Figure S3. 5%Ru/HPS 5000× magnification SEM; Figure S4. 5%Ru/HPS 10,000× magnification SEM; Figure S5. 3%Ru@0.1%Co/HPS 100× magnification SEM; Figure S6. 3%Ru@0.1%Co/HPS 3000× magnification SEM; Figure S7. 3%Ru@0.1%Co/HPS 5000× magnification SEM; Figure S8. 3%Ru@0.1%Co/HPS 10,000× magnification SEM; Figure S9. 3%Ru@0.1%Cu/HPS 100× magnification SEM; Figure S10. 3%Ru@0.1%Cu/HPS 3000× magnification SEM; Figure S11. 3%Ru@0.1%Cu/HPS 5000× magnification SEM; Figure S12. 3%Ru@0.1%Cu/HPS 10,000× magnification SEM; Figure S13. 3%Ru@0.1%Ni/HPS 100× magnification SEM; Figure S14. 3%Ru@0.1%Ni/HPS 3000× magnification SEM; Figure S15. 3%Ru@0.1%Ni/HPS 5000× magnification SEM; Figure S16. 3%Ru@0.1%Ni/HPS 10,000× magnification SEM; Figure S17. FT-IR spectrum of canola oil (red) and canola FAME (black); Figure S18. ^1H NMR spectrum of canola FAME in CDCl_3 ; Figure S19. Canola FAME GC-MS chromatogram; Table S1. List of identified compounds for the canola FAME GC-MS; Figure S20. Hydroformylated canola FAME GC-MS chromatogram; Table S2. List of identified compounds for the hydroformylated canola FAME GC-MS; Figure S21. Hydrogenated canola FAME GC-MS chromatogram; Table S3. List of identified compounds for the hydroformylated canola FAME GC-MS; Figure S22. Oxidized canola FAME GC-MS chromatogram; Table S4. List of identified compounds for the oxidized canola FAME GC-MS; Figure S23. Deoxygenated canola FAME GC-MS chromatogram. And Table S5. List of identified compounds for the deoxygenated canola FAME GC-MS.

Author Contributions: Conceptualization, M.G.S., V.G.M., S.M.P.M., M.R.M. and P.A.Z.S.; methodology, R.C.D., T.V.S.M., D.d.G.R., V.G.M., S.M.P.M., M.R.M. and P.A.Z.S.; investigation, R.C.D., T.V.S.M., D.d.G.R., V.G.M., S.M.P.M., M.R.M. and P.A.Z.S.; resources, M.G.S., V.G.M., S.M.P.M., M.R.M. and P.A.Z.S.; writing—review and editing, V.G.M., S.M.P.M., M.R.M. and P.A.Z.S.; supervision, S.M.P.M. and P.A.Z.S.; project administration, V.G.M., S.M.P.M. and P.A.Z.S.; funding acquisition, M.G.S., V.G.M., S.M.P.M., M.R.M. and P.A.Z.S. All authors have read and agreed to the published version of the manuscript.

Funding: This research was supported by the National Council for Scientific and Technological Development (CNPq)—BRICS project 442095/2017-1-Call N. 2 BRICS-STI/CNPQ, the Brazilian Federal Agency for the Improvement of Higher Education (CAPES), the Brazilian Innovation Agency (FINEP), Alagoas Research Foundation (FAPEAL) and the DF Research Foundation (FAP-DF). R.C.D., T.V.S.M. and D.G.R. express their appreciation for fellowships granted by CAPES and CNPq. S.M.P.M., M.R.M. and P.A.Z.S. thank CNPq for research fellowships.

Acknowledgments: The authors thank the LSCAT/CTEC/UFAL and GON/IF/UFAL teams for their contributions.

Conflicts of Interest: The authors declare no conflict of interest.

References

1. Poovan, F.; Chandrashekhar, V.G.; Natte, K.; Jagadeesh, R.V. Synergy between Homogeneous and Heterogeneous Catalysis. *Catal. Sci. Technol.* **2022**, *12*, 6623–6649. [[CrossRef](#)]
2. Khan, H.M.; Iqbal, T.; Yasin, S.; Irfan, M.; Abbas, M.M.; Veza, I.; Soudagar, M.E.M.; Abdelrahman, A.; Kalam, M.A. Heterogeneous Catalyzed Biodiesel Production Using Cosolvent: A Mini Review. *Sustainability* **2022**, *14*, 5062. [[CrossRef](#)]
3. Farnetti, E.; Di Monte, R.; Kašpar, J. Homogeneous and Heterogeneous Catalysis. In *Inorganic and Bio-Inorganic Chemistry*; Bertini, I., Ed.; EOLSS Publications: Abu Dhabi, United Arab Emirates, 2009; Volume 2.
4. Velenturf, A.P.M.; Purnell, P. Principles for a Sustainable Circular Economy. *Sustain. Prod. Consum.* **2021**, *27*, 1437–1457. [[CrossRef](#)]
5. Sekoai, P.T.; Ghimire, A.; Ezeokoli, O.T.; Rao, S.; Ngan, W.Y.; Habimana, O.; Yao, Y.; Yang, P.; Fung, A.H.Y.; Yoro, K.O. Valorization of Volatile Fatty Acids from the Dark Fermentation Waste Streams—A Promising Pathway for a Biorefinery Concept. *Renew. Sustain. Energy Rev.* **2021**, *143*, 110971. [[CrossRef](#)]
6. Kahar, P.; Rachmadona, N.; Pangestu, R.; Palar, R.; Adi, D.T.N.; Juanssilfero, A.B.; Manurung, I.; Hama, S.; Ogino, C. An Integrated Biorefinery Strategy for the Utilization of Palm-Oil Wastes. *Bioresour. Technol.* **2022**, *344*, 126266. [[CrossRef](#)]
7. Awogbemi, O.; Von Kallon, D.V.; Aigbodion, V.S. Trends in the Development and Utilization of Agricultural Wastes as Heterogeneous Catalyst for Biodiesel Production. *J. Energy Inst.* **2021**, *98*, 244–258. [[CrossRef](#)]
8. Behr, A.; Seidensticker, T. *Chemistry of Renewables: An Introduction*; Springer Nature: London, UK, 2020; ISBN 3662614308.
9. Jayakumar, M.; Karmegam, N.; Gundupalli, M.P.; Gebeyehu, K.B.; Asfaw, B.T.; Chang, S.W.; Ravindran, B.; Awasthi, M.K. Heterogeneous Base Catalysts: Synthesis and Application for Biodiesel Production—A Review. *Bioresour. Technol.* **2021**, *331*, 125054. [[CrossRef](#)]
10. Lin, L.; Han, X.; Han, B.; Yang, S. Emerging Heterogeneous Catalysts for Biomass Conversion: Studies of the Reaction Mechanism. *Chem. Soc. Rev.* **2021**, *50*, 11270–11292. [[CrossRef](#)]
11. Behr, A.; Gomes, J.P. The Refinement of Renewable Resources: New Important Derivatives of Fatty Acids and Glycerol. *Eur. J. Lipid Sci. Technol.* **2010**, *112*, 31–50. [[CrossRef](#)]
12. Luo, S.; Yao, J.; Wang, R.; Wang, L.; Chen, X.; Yu, D.; Elfalleh, W. Effect of Nickel Modification on Ru–Ni/NaY Catalyst Structure and Linoleic Acid Isomerization Selectivity. *J. Food Meas. Charact.* **2021**, *15*, 5584–5598. [[CrossRef](#)]
13. Strelakova, A.; Shesterkina, A.; Kustov, L. Recent Progress in Hydrogenation of Esters on Heterogeneous Bimetallic Catalysts. *Catal. Sci. Technol.* **2021**, *11*, 7229–7238. [[CrossRef](#)]
14. Liu, B.; Wang, Y.; Huang, N.; Lan, X.; Xie, Z.; Chen, J.G.; Wang, T. Heterogeneous Hydroformylation of Alkenes by Rh-Based Catalysts. *Chem* **2022**, *8*, 2630–2658. [[CrossRef](#)]
15. Rodrigues, F.M.S.; Carrilho, R.M.B.; Pereira, M.M. Reusable Catalysts for Hydroformylation-Based Reactions. *Eur. J. Inorg. Chem.* **2021**, *2021*, 2294–2324. [[CrossRef](#)]
16. Kerenkan, A.E.; Béland, F.; Do, T.-O. Chemically Catalyzed Oxidative Cleavage of Unsaturated Fatty Acids and Their Derivatives into Valuable Products for Industrial Applications: A Review and Perspective. *Catal. Sci. Technol.* **2016**, *6*, 971–987. [[CrossRef](#)]
17. Gámez, S.; de la Torre, E.; Gaigneaux, E.M. Carbon Black-Polydopamine-Ruthenium Composite as a Recyclable Boomerang Catalyst for the Oxidative Cleavage of Oleic Acid. *Chem. Eng. J.* **2022**, *427*, 131820. [[CrossRef](#)]
18. Upadhyay, R.; Rana, R.; Sood, A.; Singh, V.; Kumar, R.; Srivastava, V.C.; Maurya, S.K. Heterogeneous Vanadium-Catalyzed Oxidative Cleavage of Olefins for Sustainable Synthesis of Carboxylic Acids. *Chem. Commun.* **2021**, *57*, 5430–5433. [[CrossRef](#)] [[PubMed](#)]
19. Aiamsiri, P.; Tumnantong, D.; Yoosuk, B.; Ngamcharussrivichai, C.; Prasassarakich, P. Biohydrogenated Diesel from Palm Oil Deoxygenation over Unsupported and γ -Al₂O₃ Supported Ni–Mo Catalysts. *Energy Fuels* **2021**, *35*, 14793–14804. [[CrossRef](#)]

20. Mahdi, H.I.; Bazargan, A.; McKay, G.; Azelee, N.I.W.; Meili, L. Catalytic Deoxygenation of Palm Oil and Its Residue in Green Diesel Production: A Current Technological Review. *Chem. Eng. Res. Des.* **2021**, *174*, 158–187. [[CrossRef](#)]
21. da Costa, A.A.F.; de Oliveira Pires, L.H.; Padrón, D.R.; Balu, A.M.; da Rocha Filho, G.N.; Luque, R.; do Nascimento, L.A.S. Recent Advances on Catalytic Deoxygenation of Residues for Bio-Oil Production: An Overview. *Mol. Catal.* **2022**, *518*, 112052. [[CrossRef](#)]
22. Alsalahi, W.; Trzeciak, A.M. Rhodium-Catalyzed Hydroformylation under Green Conditions: Aqueous/Organic Biphasic, “on Water”, Solventless and Rh Nanoparticle Based Systems. *Coord. Chem. Rev.* **2021**, *430*, 213732. [[CrossRef](#)]
23. Cheng, S.; Martínez-Monteagudo, S.I. Hydrogenation of Lactose for the Production of Lactitol. *Asia-Pac. J. Chem. Eng.* **2019**, *14*, e2275. [[CrossRef](#)]
24. Sulman, M.; Doluda, V.; Grigoryev, M.; Manaenkov, O.; Filatova, A.; Molchanov, V.; Sidorov, A.; Bykov, A.; Shkileva, I.; Sulman, A. Influence of the Mesoporous Polymer Matrix Nature on the Formation of Catalytically Active Ruthenium Nanoparticles. *Bull. Chem. React. Eng. Catal.* **2015**, *10*, 313–323. [[CrossRef](#)]
25. Xu, Y.; Hua, M.; Dong, X.; Chen, C.; Duan, Y.; Tang, H. From Scrap Polystyrene Foam to Efficient Demercurizer: In-Situ Synthesis of Fe-Embedded Hyper-Cross-Linked Polymers. *Appl. Catal. B Environ.* **2021**, *285*, 119791. [[CrossRef](#)]
26. Grigorev, M.E.; Mikhailov, S.P.; Bykov, A.V.; Sidorov, A.I.; Tiamina, I.Y.; Vasiliev, A.L.; Nikoshvili, L.Z.; Matveeva, V.G.; Meneghetti, S.M.P.; Sulman, M.G. Mono-and Bimetallic (Ru-Co) Polymeric Catalysts for Levulinic Acid Hydrogenation. *Catal. Today* **2021**, *378*, 167–175. [[CrossRef](#)]
27. Nikoshvili, L.; Bakhvalova, E.S.; Bykov, A.V.; Sidorov, A.I.; Vasiliev, A.L.; Matveeva, V.G.; Sulman, M.G.; Sapunov, V.N.; Kiwi-Minsker, L. Study of Deactivation in Suzuki Reaction of Polymer-Stabilized Pd Nanocatalysts. *Processes* **2020**, *8*, 1653. [[CrossRef](#)]
28. Protsenko, I.I.; Abusuek, D.A.; Nikoshvili, L.Z.; Bykov, A.V.; Matveeva, V.G.; Sulman, E.M. The Use of the Ru-Containing Catalyst Based on Hypercrosslinked Polystyrene in the Hydrogenation of Levulinic Acid to γ -Valerolactone. *Catal. Ind.* **2018**, *10*, 301–312. [[CrossRef](#)]
29. Chew, S.C. Cold-Pressed Rapeseed (*Brassica Napus*) Oil: Chemistry and Functionality. *Food Res. Int.* **2020**, *131*, 108997. [[CrossRef](#)] [[PubMed](#)]
30. Noda, L.K.; de Almeida, R.M.; Gonçalves, N.S.; Probst, L.F.D.; Sala, O. TiO₂ with a High Sulfate Content—Thermogravimetric Analysis, Determination of Acid Sites by Infrared Spectroscopy and Catalytic Activity. *Catal. Today* **2003**, *85*, 69–74. [[CrossRef](#)]
31. Noda, L.K.; de Almeida, R.M.; Probst, L.F.D.; Gonçalves, N.S. Characterization of Sulfated TiO₂ Prepared by the Sol–Gel Method and Its Catalytic Activity in the *n*-Hexane Isomerization Reaction. *J. Mol. Catal. A Chem.* **2005**, *225*, 39–46. [[CrossRef](#)]
32. Rojas, J.V.; Toro-Gonzalez, M.; Molina-Higgins, M.C.; Castano, C.E. Facile Radiolytic Synthesis of Ruthenium Nanoparticles on Graphene Oxide and Carbon Nanotubes. *Mater. Sci. Eng. B* **2016**, *205*, 28–35. [[CrossRef](#)]
33. Nikoshvili, L.Z.; Protsenko, I.I.; Abusuek, D.A.; Zaykovskaya, A.O.; Bykov, A.V.; Matveeva, V.; Sulman, E. Hydrogenation of Biomass-Derived Levulinic Acid to Gamma-Valerolactone Using Polymer-Based Metal-Containing Catalysts. *Chem. Eng. Trans.* **2017**, *61*, 895–900. [[CrossRef](#)]
34. Dunn, R.O. Correlating the Cloud Point of Biodiesel with Its Fatty Acid Methyl Ester Composition: Multiple Regression Analyses and the Weighted Saturation Factor (WSF). *Fuel* **2021**, *300*, 120820. [[CrossRef](#)]
35. Zuin, V.G.; Eilks, I.; Elschami, M.; Kümmerer, K. Education in Green Chemistry and in Sustainable Chemistry: Perspectives towards Sustainability. *Green Chem.* **2021**, *23*, 1594–1608. [[CrossRef](#)]
36. Barton, A.F.M. *Handbook of Polymer-Liquid Interaction Parameters and Solubility Parameters*; Routledge: Oxfordshire, UK, 2018; Volume 1, p. 297, ISBN 0203752619.
37. Cizmeçi, M.; Musavi, A.; Tekin, A.; Kayahan, M. Catalytic Behavior of Ruthenium in Soybean Oil Hydrogenation. *Eur. J. Lipid Sci. Technol.* **2009**, *111*, 607–611. [[CrossRef](#)]
38. Madureira, A.; Noël, S.; Léger, B.; Ponchel, A.; Monflier, E. Catalytic Hydrogenation of Derived Vegetable Oils Using Ion-Exchange Resin-Supported Ruthenium Nanoparticles: Scope and Limitations. *ACS Sustain. Chem. Eng.* **2022**, *10*, 16588–16597. [[CrossRef](#)]
39. Sarno, M.; Iuliano, M.; Viscusi, G.; Zarli, A.; Ciambelli, P. A Nickel/Palladium/Ruthenium–Graphene Based Nanocatalyst for Selective Catalytic Hydrogenation of Vegetable Oils. *Ind. Crop. Prod.* **2021**, *170*, 113815. [[CrossRef](#)]
40. Ho, C.-M.; Yu, W.-Y.; Che, C.-M. Ruthenium Nanoparticles Supported on Hydroxyapatite as an Efficient and Recyclable Catalyst for Dihydroxylation and Oxidative Cleavage of Alkenes. *Angew. Chem. Int. Ed.* **2004**, *43*, 3303–3307. [[CrossRef](#)]
41. Gámez, S.; Magerat, A.; de la Torre, E.; Gaigneaux, E.M. Functionalization of Carbon Black for Ru Complexation Towards the Oxidative Cleavage of Oleic Acid. *SSRN Electron. J.* **2022**. [[CrossRef](#)]
42. Stepacheva, A.A.; Sidorov, A.I.; Matveeva, V.G.; Sulman, M.G.; Sulman, E.M. Fatty Acid Deoxygenation in Supercritical Hexane over Catalysts Synthesized Hydrothermally for Biodiesel Production. *Chem. Eng. Technol.* **2019**, *42*, 780–787. [[CrossRef](#)]
43. Xu, G.; Zhang, Y.; Fu, Y.; Guo, Q. Efficient Hydrogenation of Various Renewable Oils over Ru-HAP Catalyst in Water. *ACS Catal.* **2017**, *7*, 1158–1169. [[CrossRef](#)]
44. Konwar, L.J.; Oliani, B.; Samikannu, A.; Canu, P.; Mikkola, J.-P. Efficient Hydrothermal Deoxygenation of Tall Oil Fatty Acids into *n*-Paraffinic Hydrocarbons and Alcohols in the Presence of Aqueous Formic Acid. *Biomass Convers. Biorefinery* **2022**, *12*, 51–62. [[CrossRef](#)]
45. Mondal, S.; Singuru, R.; Chandra Shit, S.; Hayashi, T.; Irle, S.; Hijikata, Y.; Mondal, J.; Bhaumik, A. Ruthenium Nanoparticle-Decorated Porous Organic Network for Direct Hydrodeoxygenation of Long-Chain Fatty Acids to Alkanes. *ACS Sustain. Chem. Eng.* **2018**, *6*, 1610–1619. [[CrossRef](#)]

46. Ramalho, H.F.; di Ferreira, K.M.C.; Machado, P.M.A.; Oliveira, R.S.; Silva, L.P.; Prauchner, M.J.; Suarez, P.A.Z. Biphasic Hydroformylation of Soybean Biodiesel Using a Rhodium Complex Dissolved in Ionic Liquid. *Ind. Crop. Prod.* **2014**, *52*, 211–218. [[CrossRef](#)]
47. Corradini, S.A.d.S.; Lenzi, G.G.; Lenzi, M.K.; Soares, C.M.F.; Santos, O.A.A. Characterization and Hydrogenation of Methyl Oleate over Ru/TiO₂, Ru–Sn/TiO₂ Catalysts. *J. Non. Cryst. Solids* **2008**, *354*, 4865–4870. [[CrossRef](#)]
48. Alvila, L.; Pakkanen, T.A.; Krause, O. Hydroformylation of Olefins Catalysed by Supported Ru₃(CO)₁₂ with 2, 2'-Bipyridine or with Other Heterocyclic Nitrogen Base. *J. Mol. Catal.* **1993**, *84*, 145–156. [[CrossRef](#)]
49. Oresmaa, L.; Moreno, M.A.; Jakonen, M.; Suvanto, S.; Haukka, M. Catalytic Activity of Linear Chain Ruthenium Carbonyl Polymer [Ru (CO) 4] n in 1-Hexene Hydroformylation. *Appl. Catal. A Gen.* **2009**, *353*, 113–116. [[CrossRef](#)]
50. Ungvary, F. Application of Transition Metals in Hydroformylation. Annual Survey Covering the Year 1995. *Coord. Chem. Rev.* **1997**, *160*, 129–159. [[CrossRef](#)]
51. Zimmermann, F.; Meux, E.; Mieloszynski, J.-L.; Lecuire, J.-M.; Oget, N. Ruthenium Catalysed Oxidation without CCl₄ of Oleic Acid, Other Monoenic Fatty Acids and Alkenes. *Tetrahedron Lett.* **2005**, *46*, 3201–3203. [[CrossRef](#)]
52. Chen, J.; Xu, Q. Hydrodeoxygenation of Biodiesel-Related Fatty Acid Methyl Esters to Diesel-Range Alkanes over Zeolite-Supported Ruthenium Catalysts. *Catal. Sci. Technol.* **2016**, *6*, 7239–7251. [[CrossRef](#)]
53. Krishnapriya, R.; Gupta, U.; Soni, V.K.; Sharma, R.K. Catalytic Conversion of Methyl Oleate to Hydrocarbons: Impact of Cobalt Oxide Species Integration in SiO₂–Al₂O₃. *Sustain. Energy Fuels* **2020**, *4*, 3308–3317. [[CrossRef](#)]
54. Mendes, A.N.F.; Gregório, J.R.; da Rosa, R.G. Studies on the Experimental Variables Effects on Rhodium Catalyzed Hydroformylation of Unsaturated Fatty Esters and Comparison of [RhH(CO)(PPh₃)₃] and [RhCl₃.3H₂O] as Starting Catalytic Precursors. *J. Braz. Chem. Soc.* **2005**, *16*, 1124–1129. [[CrossRef](#)]
55. Ramalho, H.F.; Ferreira, K.M.C.; Machado, P.M.A.; Silva, T.B.; Rangel, E.T.; Prauchner, M.J.; Suarez, P.A.Z. Production of Additives with Antimicrobial Activity via Tandem Hydroformylation-Amine Condensation of Soybean FAME Using an Ionic Liquid-Based Biphasic Catalytic System. *J. Braz. Chem. Soc.* **2015**, *27*, 321–333. [[CrossRef](#)]

Disclaimer/Publisher's Note: The statements, opinions and data contained in all publications are solely those of the individual author(s) and contributor(s) and not of MDPI and/or the editor(s). MDPI and/or the editor(s) disclaim responsibility for any injury to people or property resulting from any ideas, methods, instructions or products referred to in the content.